Available online at www.sciencedirect.com

SciVerse ScienceDirect

Nuclear Physics B 854 [FS] (2012) 166–183

NUCLEAR PHYSICS B

www.elsevier.com/locate/nuclphysb

Simplicial gauge theory and quantum gauge theory simulation

Tore Gunnar Halvorsen [a], Torquil Macdonald Sørensen [b,*]

[a] *Department of Mathematical Sciences, Norwegian University of Science and Technology, NO-7491 Trondheim, Norway*

[b] *Centre of Mathematics for Applications, University of Oslo, NO-0316 Oslo, Norway*

Received 8 July 2011; accepted 17 August 2011

Available online 24 August 2011

Abstract

We propose a general formulation of simplicial lattice gauge theory inspired by the finite element method. Numerical tests of convergence towards continuum results are performed for several $SU(2)$ gauge fields. Additionally, we perform simplicial Monte Carlo quantum gauge field simulations involving measurements of the action as well as differently sized Wilson loops as functions of β.

MSC: 35Q40; 74S05; 81T13; 81T25

Keywords: Lattice gauge theory; QCD; Finite element method; Simplicial mesh; Yang–Mills action

1. Introduction

1.1. General introduction

Gauge quantum field theory (QFT) has been extremely successful in modeling the behaviour of fundamental high energy particle physics. This is done using the standard model of particle physics, which is based on the gauge symmetry group $\mathcal{G} = U(1) \times SU(2) \times SU(3)$. Quantum gauge field theories based on such noncommutative gauge groups are also called Yang–Mills

* Corresponding author.
E-mail addresses: toregha@gmail.com (T.G. Halvorsen), t.m.sorensen@matnat.uio.no, torquil@gmail.com (T.M. Sørensen).

0550-3213/$ – see front matter
doi:10.1016/j.nuclphysb.2011.08.016

theories [1–4]. Despite the massive successes of this model, there are still large difficulties in calculating low energy properties of quarks and gluons. When restricting to these quantum fields, the standard model reduces to the theory of Quantum Chromodynamics (QCD), with gauge group $SU(3)$. The problems is that through the effect of renormalization, the QCD coupling constant increases as interaction energies is decrease, in such a way that perturbation theory breaks down. This phenomenon is the source of confinement in QCD. Direct paper-and-pen calculation of masses and interactions among low energy bound states of quarks is therefore quite problematic.

1.2. Lattice gauge theory

By discretizing QCD onto a lattice, a lot of these difficulties are removed. Lattice gauge theory (LGT) [5,6] has proven itself to be a powerful method of doing nonperturbative gauge theory calculations. It has therefore been, still is, and will for a long time be immensely useful in testing QCD against experimental results at low energy.

Usually LGT models are formulated using a hypercubic lattice on a Euclidean spacetime. Such a mesh preserves some discrete subgroups of the translational, mirror and 4d rotational symmetries. Note that a clever way of retaining continuous symmetries while working on a lattice is to use random lattices [7–9].

The models are almost always defined so as to also preserve a discrete gauge symmetry. This has the beneficial effect of enforcing a vanishing gluon mass in the discrete model.

1.3. Simplicial lattices

Simplicial meshes have been used for QCD simulations before [10–16], with promising numerical results. Here, we construct a simplicial gauge theory (SGT) based on the general mathematical concept of a simplicial complex, while preserving gauge invariance. This allows us to define SGT on a very general class of meshes, without restricting ourselves to a particular type of simplicial lattice.

The construction of the gauge invariant SGT action functional is inspired by the finite element method (FEM) most commonly used for solving partial differential equations, particularly on complicated domains [17–21]. The formalism therefore includes the use of finite element function spaces on simplicial meshes, and the concept of mass matrices. The term "mass matrix" in this context has nothing to do with physical particle masses, and is therefore not to be confused with the usual mass matrix of quantum states within quantum field theory.

Through the use of the FEM formulation, and the massive resources of methods available within that subject area, we hope to gain advantages for QCD simulations in future implementations, in particular with regards to the possibilities of grid refinement. This could be useful in modeling some QCD phenomena, e.g. for highly concentrated gluon flux tubes between quarks where an increase lattice resolution might be desired. An earlier work used FEM inspired methods within QFT, although along a different direction involving solutions of operator equations instead of Monte Carlo simulations [22,23].

1.4. Computer simulation

The mathematical proof of consistency between the SGT and continuous Yang–Mills gauge theory action is described in a companion paper [24], along with a description of the more comprehensive Yang–Mills–Higgs model. In the current article we are content to provide numerical

evidence for convergence towards exact continuum results for several choices of gauge field configurations. In addition, we perform Monte Carlo quantum pure gauge field theory simulations for the gauge group $SU(2)$ in temporal gauge, as a proof-of-concept for SGT. Observable measurements include expectation values of the action density as well as a series of different Wilson loops.

1.5. Outline

Section 2 contains a short repetition of the fundamental definitions of gauge symmetry and the continuous spacetime Yang–Mills action in Section 2.1, the basics of traditional lattice gauge theory in Section 2.2, as well as an introduction to the proposed SGT action in Section 2.3. In Section 3.1, we report on the numerical convergence of the SGT action towards the exact continuum value for several different cases of $SU(2)$ gauge fields, as well as similar results from traditional LGT. Theoretical results proving consistency for general gauge fields can be found in [24]. In Section 3.2, we perform Monte Carlo quantum field theory simulations in order to observe that SGT correctly reproduces the basic aspects of the $SU(2)$ quantum field theory. We draw our conclusions in Section 4. Appendix A contains a short introduction to elementary aspects of simplicial complexes, and some notes about basis functions and mass matrices that are use in our construction of SGT. Appendix B contains a calculation of strong and weak coupling limits for a Wilson triangle and the action density. Lastly, Appendix C contains a short discussion of some aspects of the numerical computer implementation.

2. Construction

2.1. Continuous gauge theory

Consider the spacetime domain $\mathbb{M} = \mathbb{R} \times S$, where $\mathbb{R}$ is time and $S \subset \mathbb{R}^3$. The domain $\mathbb{M}$ represents either Lorentzian or Euclidean spacetime, in each case equipped with the appropriate metric. In the standard orthonormal $\mathbb{M}$-basis $\{e_\mu\}_{\mu=0,1,2,3}$, a general point $x \in \mathbb{M}$ has components $\{x^\mu\}_{\mu=0,1,2,3}$. Greek indices run from 0 to 3, and Latin indices from 1 to 3.

Furthermore, in this article we shall consider pure $SU(2)$ gauge theory. However, the construction presented is applicable to any gauge theory based on a compact Lie group $\mathcal{G}$ which can be represented by a subgroup of the complex unitary $n \times n$ matrices. We define the real-valued scalar product on $\mathcal{G}$ as

$$g' \cdot g := \Re \operatorname{tr}\left(g' g^H\right), \tag{1}$$

where g^H is the hermitian conjugate of a matrix g.

The connection between the continuous theory and the discrete simplicial theory is most easily seen in a coordinate free formulation. Thus, we start with a coordinate free formulation, before we give the more familiar coordinate based one.

The free variable in pure Yang–Mills theory with gauge Lie group $\mathcal{G}$ is a gauge potential or more formally a one-form A on $\mathbb{M}$, with values in the corresponding gauge Lie algebra $\mathfrak{g}$. For simplicity of notation, we hereby specify $\mathcal{G} = SU(2)$ and $\mathfrak{g} = \mathfrak{su}(2)$. We split A into temporal and spatial components $A = (A_0, \mathbf{A})$. In this context, A_0 can be thought of as a scalar function,[1] and $\mathbf{A}$ as a spatial vector. The curvature (field strength) of such a one-form is given by

[1] However, not a scalar in the sense of spacetime symmetry transformation properties.

$$F(A) = \mathbb{d}A + \frac{i}{2}[A, A] = d_0\mathbf{A} + dA_0 + d\mathbf{A} + i[\mathbf{A}, A_0] + \frac{i}{2}[\mathbf{A}, \mathbf{A}], \tag{2}$$

where $\mathbb{d} = (d_0, d)$, d_0 and d denote exterior derivative in the temporal and spatial directions respectively, and $[\cdot,\cdot]$ is the commutator between Lie algebra valued one-forms. We choose the basis $\{t^a\}_{a=1,2,3}$, where $t^a := \sigma^a/2$, for $\mathfrak{su}(2)$, where $\{\sigma^a\}_{a=1,2,3}$ are the Pauli matrices. Thus, we can expand the gauge field into components, $A = A^a t^a$. We also have

$$[A, A] = \sum_{ab} A^a \wedge A^b \big[t^a, t^b\big] = \sum_{abc} i\varepsilon^{abc} A^a \wedge A^b t^c, \tag{3}$$

where ε^{abc} is the antisymmetric Levi-Civita symbol with $\epsilon^{123} = 1$ and $\wedge$ is the wedge product (exterior product). For later convenience we split the curvature in a temporal and spatial part

$$F^t(A) = d_0\mathbf{A} + dA_0 + i[\mathbf{A}, A_0], \qquad F^s(A) = d\mathbf{A} + \frac{i}{2}[\mathbf{A}, \mathbf{A}]. \tag{4}$$

The action that defines the gauge theory is the functional

$$S[A] = \frac{1}{4e^2}\int_{\mathbb{M}} \big|F(A)\big|^2 = \frac{1}{4e^2}\int_{\mathbb{M}} \big|F^t(A)\big|^2 + \big|F^s(A)\big|^2, \tag{5}$$

where the norms are generated the metric and e is the dimensionless Yang–Mills coupling constant.

A gauge transformation is defined by a choice of $G(x) \in SU(2)$ for each $x \in \mathbb{M}$, and transforms the gauge field as

$$A_0 \mapsto G(A_0 + d_t)G^{-1}, \qquad \mathbf{A} \mapsto G(\mathbf{A} + d)G^{-1}. \tag{6}$$

Note that the action $S[A]$ is invariant under such gauge transformations. For a more precise mathematical exposition, see [24].

A formulation more familiar within physics is obtained by expressing the one form and curvature in coordinates. In other words, one decomposes the one-form A^a in the basis $\{dx^\mu\}$, i.e. $A^a = \sum_\mu A^a_\mu\, dx^\mu$. The exterior derivative of such a one-form is given by

$$\mathbb{d}A^a = \sum_{\mu\nu} \partial_\nu A^a_\mu\, dx^\nu \wedge dx^\mu = \sum_{\mu\nu} \frac{1}{2}\big(\partial_\mu A^a_\nu - \partial_\nu A^a_\mu\big)\, dx^\mu \wedge dx^\nu. \tag{7}$$

Furthermore, the curvature is given by $F^a = \sum_{\mu\nu} \frac{1}{2} F^a_{\mu\nu}\, dx^\mu \wedge dx^\nu$, where

$$F^a_{\mu\nu} = \partial_\mu A^a_\nu - \partial_\nu A^a_\mu - \varepsilon^{abc} A^b_\mu A^c_\nu. \tag{8}$$

Finally, the action can be expressed as

$$S = \frac{1}{4e^2}\int_{\mathbb{M}} \sum_{\mu\nu a} F^a_{\mu\nu} F^{a\mu\nu}\, dx, \tag{9}$$

the usual coordinate dependent expression for the Yang–Mills action functional.

2.2. Lattice gauge theory

To see the connection between lattice gauge theory (LGT) and the simplicial gauge theory (SGT), we will in this section give a brief overview of the discretization procedure from LGT. For a more complete description see e.g. [6].

The discretization procedure of both LGT and SGT is based on the following identity. Consider a small surface Σ with area proportional to h^2, where h is a small positive quantity. Then the following identity holds

$$\oiint_{\Sigma} F(A) = \mathcal{H}(A) - 1 + \mathcal{O}\big(h^3\big),$$

where $\mathcal{H}(A)$ is the holonomy of the one-form A, i.e. the parallel transport induced by A around the boundary of Σ. This parallel transport is defined as follows. Given a curve $\gamma : [0,1] \to \mathbb{M}$, such that $\gamma(0) = x$ and $\gamma(1) = y$, the parallel transport operator along γ is given by

$$U_\gamma(x,y) = P\left(\exp\left(i \int_\gamma A\right)\right),$$

where P denotes path-ordering, and the subscript γ is attached to U to denote the path-dependence. In LGT, this quantity is known as the Wilson line.

In LGT, spacetime $\mathbb{M}$ is usually discretized by a uniform hypercubic lattice $\mathbb{L}$. Neighbouring node positions are related through translation vectors $\{a_\mu\}$ for which we assume $|a_\mu| = h$ for all μ. To each edge e which connects neighbouring nodes, n and $n + a_\mu$ for some μ, we attach an approximation of the parallel transport operator along e. Thus,

$$U_\mu(n) := \exp\left(ihA_\mu\left(n + \frac{1}{2}a_\mu\right)\right) \approx U_e(n, n+a_\mu) = P\left(\exp\left(i \int_n^{n+a_\mu} A\right)\right). \tag{10}$$

In LGT this quantity is called a link variable, link matrix or link group element. Furthermore, given a face f of a cube in the mesh, called a plaquette, we approximate the holonomy associated to this face as the path-ordered product of the link variables along its boundary. In other words, if f lies in the $\mu\nu$ plane, with nodes n, $n + a_\mu$, $n + a_\nu$, and $n + a_\mu + a_\nu$, we approximate the holonomy as

$$\begin{aligned} U_f(n) &:= U_{\mu\nu}(n) := U_\mu(n) U_\nu(n + a_\mu) U_\mu^H(n + a_\nu) U_\nu^H(n) \\ &\approx \mathcal{H}(A) := P\left(\exp\left(i \oint_{\partial f} A\right)\right), \end{aligned} \tag{11}$$

where ∂f denotes the boundary of the plaquette f. In LGT, this quantity is known as the Wilson loop. Moreover, we approximate the curvature as

$$F_{\mu\nu}^f \approx U_f - \mathbb{1}. \tag{12}$$

Finally, the LGT action is defined as

$$S_{LGT} = \beta \sum_f \frac{1}{4} \operatorname{tr}\big[(U_f - \mathbb{1})(U_f - \mathbb{1})^H\big] = \beta \sum_f 1 - \frac{1}{4} \operatorname{tr}\big(U_f + U_f^H\big), \tag{13}$$

where β is related to the coupling constant by $\beta = 4/e^2$. A discrete gauge transformation is associated with a choice of $G(n) \in SU(2)$ for each node n. Each link variable then transforms as

$$U_\mu(n) \mapsto G(n)U_\mu(n)G(n+a_\mu)^{-1}. \tag{14}$$

By the cyclic invariance of the trace, the action S_{LGT} is discretely gauge invariant.

2.2.1. Remarks

The LGT action can be viewed as a mass lumped FEM action, and this observation is useful to have in mind when we construct the simplicial analogue. In the FEM setting, the gauge potential is assumed to be a lowest order curl-conforming Nédélec element in 4d on hypercubes, with one dimension representing time [19]. The degree of freedom associated to such a gauge potential at an edge e from n to $n+a_\mu$ is

$$A_e = \int_n^{n+a_\mu} A = hA_\mu\left(n + \frac{1}{2}a_\mu\right).$$

The parallel transport operator is as in Eq. (10), i.e. $U_\mu(n) = \exp(iA_e)$. Then, the holonomy is approximated as in Eq. (11), the curvature as in Eq. (12), and one considers $U_f - \mathbb{1}$ as the components of the two-form

$$\sum_f (U_f - \mathbb{1})\omega_f,$$

where $\{\omega_f\}$ are the Nédélec basis two-forms. The FEM action associated to such a two-form is

$$S := \frac{\beta}{2}\sum_{f,f'} M_{ff'}\,\mathrm{tr}\big[(U_f - \mathbb{1})(U_{f'} - \mathbb{1})^H\big], \quad M_{ff'} := \int_{\mathbb{M}} \omega_f \cdot \omega_{f'},$$

where $M_{ff'}$ is called the mass matrix, and $(\cdot)$ denotes the scalar product of alternating forms w.r.t. the metric. The mass matrix is not diagonal, which means that the discrete curvature at different faces interact. This again implies that the action is not discretely gauge invariant. However, by diagonalizing the mass matrix using numerical quadrature, this action reduces to the LGT action, Eq. (13). The diagonalization procedure can also be shown to be numerically consistent in the sense of approximation theory [24].

2.3. Simplicial gauge theory

In this section we construct the discretely gauge invariant simplicial gauge theory (SGT) action on a simplicial complex, as defined in Appendix A. The construction is the simplicial analogue of the FEM action described above, including additional parallel transport operators to make it discretely gauge invariant.

The curvature associated to the temporal and spatial faces is defined exactly as in LGT. In the notation of Appendix A, consider a temporal and spatial face

$$\begin{aligned} f_t(\tau) &:= \{i_\tau, j_\tau, j_{\tau+\Delta t}, i_{\tau+\Delta t}\}, \\ f(\tau) &:= \{i_\tau, j_\tau, k_\tau\}, \end{aligned} \tag{15}$$

where i_τ denotes node i at time τ. The time-dependency will from here on often be suppressed, unless confusion can arise. The spatial and temporal holonomies associated to these faces, induced by the gauge potential, are approximated as

$$\begin{aligned} U_{f_t}(i_\tau) &= U(i_\tau, j_\tau)U(j_\tau, j_{\tau+\Delta t})U(j_{\tau+\Delta t}, i_{\tau+\Delta t})U(i_{\tau+\Delta t}, i_\tau), \\ U_f(i) &= U(i,j)U(j,k)U(k,i), \end{aligned} \tag{16}$$

where the arguments i_τ and i are included to indicate where the holonomy is located, and the parallel transport operators are defined exactly as in LGT, i.e. Eq. (10). We observe that the holonomies located at different nodes are related through the formulas

$$\begin{aligned} U_{f_t}(i_\tau + \Delta t) &= U(i_{\tau+\Delta t}, i_\tau)U_{f_t}(i_\tau)U(i_\tau, i_{\tau+\Delta t}), \\ U_f(j) &= U(j,i)U_f(i)U(i,j), \end{aligned}$$

which give formulas for parallel transport of curvature. Hence, we have defined the curvature associated to the temporal and spatial faces in our 4d mesh. The distinguished point of f and f_t, i.e. the location of their holonomy, are denoted $\dot{f}$ and $\dot{f}_t$ respectively. Note that under a discrete gauge transformation, the parallel transport operators are transformed as in LGT, i.e.

$$\begin{aligned} U(i_\tau, i_{\tau+\Delta t}) &\mapsto G(i_\tau)U(i_\tau, i_{\tau+\Delta t})G(i_{\tau+\Delta t})^{-1}, \\ U(i,j) &\mapsto G(i)U(i,j)G(j)^{-1}, \end{aligned}$$

for $G(i) \in SU(2)$ for each vertex i.

As in LGT the curvature is approximated as

$$\begin{aligned} F^t &\approx U_{f_t} - \mathbb{1}, \\ F^s &\approx U_f - \mathbb{1}, \end{aligned} \tag{17}$$

considered as components of the two-forms

$$\begin{aligned} &\sum_{f_t} (U_{f_t} - \mathbb{1})\Lambda_{f_t}, \\ &\sum_{f} (U_f - \mathbb{1})\Lambda_f, \end{aligned}$$

where the Λ are basis functions as described in Appendix A. The associated FEM action is $S = S_t + S_s$, where the temporal part is

$$S_t = \frac{\beta}{2}\Re \sum_{f_t, f_t'} M_{f_t f_t'} \operatorname{tr}\big[(U_{f_t} - \mathbb{1})(U_{f_t'} - \mathbb{1})^H\big], \quad M_{f_t f_t'} := \int_{\mathbb{M}} \Lambda_{f_t} \cdot \Lambda_{f_t'}, \tag{18}$$

and the spatial part is

$$S_s = \frac{\beta}{2}\Re \sum_{f, f'} M_{ff'} \operatorname{tr}\big[(U_f - \mathbb{1})(U_{f'} - \mathbb{1})^H\big], \quad M_{ff'} := \int_{\mathbb{M}} \Lambda_f \cdot \Lambda_{f'}, \tag{19}$$

where $\beta = 2/e^2$. Note that we have suppressed the dependency of S on A. Again, $M_{f_t f_t'}$ and $M_{ff'}$ are called mass matrices. They depend on the details of the mesh, and are described more in detail in Appendix A. As pointed out in the discussion about the FEM formulation of LGT, the mass matrices are not diagonal. This implies that the action is not discretely gauge invariant. However, this can be resolved by parallel transport of curvature. The temporal and spatial part of the action, S_t and S_s, are now treated separately.

2.3.1. The temporal part

Let $f_t(\tau)$ and $f'_t(\tau)$ be two temporal faces. We now use some properties of the basis functions, which are explained in Appendix A. Since the temporal basis face functions (Λ_{f_t}) are piecewise constant in time, the interactions between the temporal curvature occur only at coinciding time intervals. Also, by properties of the edge basis functions (λ_e), which define the temporal basis face functions, we can connect the curvature at f_t with the curvature at f'_t by parallel transport along at most one edge. Thus, we connect the curvatures by parallel transport along the connecting edge $e = \{\dot{f}_t, \dot{f}'_t\}$ of their distinguished points. In other words, we approximate the temporal part of the action by

$$S^t_{SGT} := \frac{\beta}{2}\Re \sum_{f_t(\tau), f'_t(\tau)} M_{f_t(\tau), f'_t(\tau)} \operatorname{tr}\big[U\big(\dot{f}'_t, \dot{f}_t\big)(U_{f_t(\tau)} - \mathbb{1})U\big(\dot{f}_t, \dot{f}'_t\big)(U_{f'_t(\tau)} - \mathbb{1})^H\big]. \tag{20}$$

2.3.2. The spatial part

Let f and f' be two spatial faces of a tetrahedron T. The curvature associated to the face f at time τ will interact with the curvature associated to the face f' not only at time τ, but also at times $\tau \pm \Delta t$, since the facial basis functions are piecewise affine in time. Thus, to connect the curvature at $f(\tau)$ with the curvature at $f'(\tau')$ we must parallel transport in both space and time. Thus, we replace

$$(U_{f(\tau)} - \mathbb{1})(U_{f'(\tau')} - \mathbb{1})^H$$

by

$$U\big(\dot{f}'(\tau), \dot{f}(\tau)\big)(U_{f(\tau)} - \mathbb{1})U\big(\dot{f}(\tau), \dot{f}'(\tau)\big)U\big(\dot{f}'(\tau), \dot{f}'\big(\tau'\big)\big)(U_{f'(\tau')} - \mathbb{1})^H \times U\big(\dot{f}'\big(\tau'\big), \dot{f}'(\tau)\big)$$

in the FEM action (19). In words, we first parallel transport the curvature associated to f, located at the vertex $\dot{f}(\tau))$ to the vertex $\dot{f}'(\tau)$ along the edge $e = \{\dot{f}(\tau), \dot{f}'(\tau)\}$. Then we parallel transport it in the temporal direction from $\dot{f}'(\tau)$ to $\dot{f}'(\tau')$. So, we approximate the spatial part of the action as

$$S^s_{SGT} := \frac{\beta}{2}\Re \sum_{f(\tau), f'(\tau')} M_{f(\tau), f'(\tau')} \operatorname{tr}\big[U\big(\dot{f}'(\tau), \dot{f}(\tau)\big)(U_{f(\tau)} - \mathbb{1})U\big(\dot{f}(\tau), \dot{f}'(\tau)\big) \times U\big(\dot{f}'(\tau), \dot{f}'\big(\tau'\big)\big)(U_{f'(\tau')} - \mathbb{1})^H U\big(\dot{f}'\big(\tau'\big), \dot{f}'(\tau)\big)\big]. \tag{21}$$

The simplicial gauge theory action is then defined as

$$S_{SGT} := S^t_{SGT} + S^s_{SGT}, \tag{22}$$

and by the cyclic invariance of the trace, this action is discretely gauge invariant. A companion paper [24] contains more details about this construction, as well as mathematical proofs of consistency with the continuous action (5) in the sense of approximation theory.

3. Computer simulation

For our SGT computer simulations, we chose the Euclidean cubic domain $\mathbb{M} = [0, 1]^4 \subset \mathbb{R}^4$ with periodic boundary conditions. We simulated the pure gauge SGT action (22) in temporal

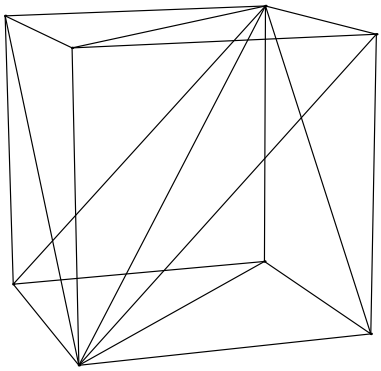

Fig. 1. Elementary 3d mesh building block containing six tetrahedra, all of which share the single interior diagonal. This particular choice implies an anisotropy in the discretization. This anisotropy will of course disappear in the continuum limit.

gauge on a simplicial lattice with the gauge group $SU(2)$. Choice of gauge is not necessary, but it does simplify the algorithm slightly, since all temporal edge matrices then reduce to the identity.

The spatial lattice was constructed using a cubic arrangement of N^3 identical building block cubes of size h^3, each consisting of six tetrahedra as shown in Fig. 1. The resulting spatial mesh was repeated at N consecutive time steps to form a cubic domain of physical volume $(hN)^4$. As described above, each spatial edge is part of two temporal square-shaped faces, going forward and backward in time.

The SGT action employs parallel transport matrices in order for gauge invariance to be respected. By defining the distinguished points of all spatial and temporal faces to coincide for as many pairs of faces as possible, we only need the parallel transport matrices for terms in the action involving pairs of temporal faces with no common nodes. More details regarding the exact computer implementation are given in Appendix C.

3.1. Convergence of the action

In order to check the continuum limit of the discrete action, we examined four different gauge field configurations for which the exact continuum value S_{cont} of the action is calculable. We did numerical calculations for square meshes with $N = 4, 8, 16, 32$ in order to observe convergence of the numerical values towards the exact values. By the estimates in [24] we expect that the error be of second order in the lattice constant h. We used the following gauge field configuration cases:

1. Gauge field oriented towards the x-direction in space and towards t^3 within $\mathfrak{su}(2)$, with a sinusoidal t-dependence. The only nonzero component of the gauge field A is
$$A_x^3(t,x,y,z) := \frac{e}{2\pi}\sin(2\pi t), \qquad S = 1.$$
2. Gauge field oriented towards the y-direction in space and t^3 within $\mathfrak{su}(2)$, with a sinusoidal x-dependence. The nonzero component of the gauge field in this case was
$$A_y^3(t,x,y,z) := \frac{e}{2\pi}\sin(2\pi x), \qquad S = 1.$$

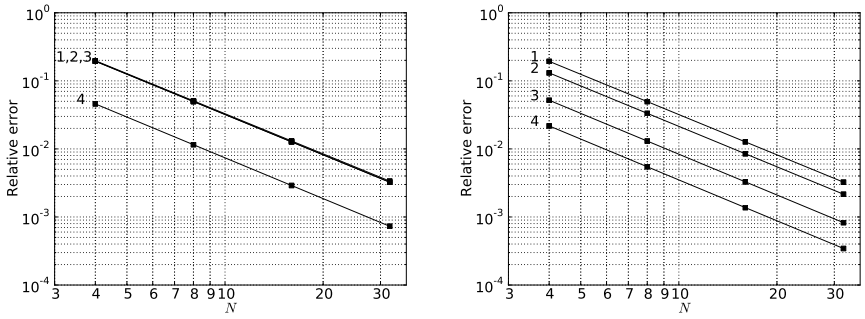

(a) LGT (b) SGT

Fig. 2. The relative error of the action versus the number of lattice sites per side N, for the actions 1, 2, 3, 4 described in Section 3.1. The squares are the simulation data points and the solid lines are the second order polynomial fits. Errors are proportional to h^2 in all cases.

3. A case with two nonzero components,

$$A_x^1 := \frac{e}{2\pi}\sin(2\pi y), \qquad A_y^2 := \frac{e}{2\pi}\sin(2\pi x), \qquad S = \frac{1}{2} + \frac{e^2}{8(2\pi)^4}.$$

4. A constant field that only contributes to the nonlinear term in the field strength,

$$A_x^1 := \sqrt{e}, \qquad A_y^2 := \sqrt{e}, \qquad S = \frac{1}{2}.$$

In order to provoke a sizable nonlinear contribution in case 3, we chose a small $\beta = 2/e^2 = 1/5$. The link matrices needed to evaluate the SGT action are calculated from these gauge fields by means of the exponential map (10).

The results are displayed using double logarithmic plots in Fig. 2 for traditional Wilson action LGT as well as the SGT results. As expected from the estimates in [24], in all cases the relative error behaves as

$$\text{Relative error} \sim Ch^2,$$

as determined by extracting the linear coefficient of the second order polynomial fits shown in the figures. Note that while the convergence exponent of h is the same in all cases, the prefactor C is smaller in the SGT cases involving time-independent fields, due to its finer spatial discretization for the same N. Where time-dependence is involved, the errors coincide since the time-discretization we have chosen for this SGT simulation is of the same quality as for the LGT simulation.

3.2. *Quantum field simulation*

Analogous to the traditional lattice QCD simulations, we performed parallel $SU(2)$ quantum field theory Monte Carlo simulations for $N = 8$. In this case, the edge matrices are sampled directly without reference to a gauge field and lattice constant value. Therefore, the physical size of the simulation domain is unknown prior to experimental comparisons. All dimensional observable quantities are automatically calculated in units of powers of the lattice constant h.

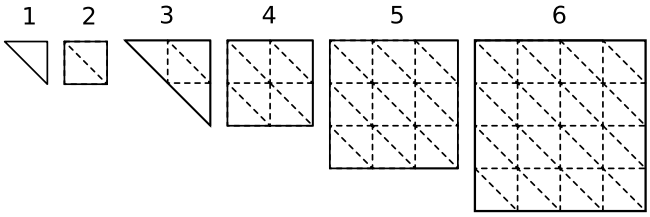

Fig. 3. The simulated Wilson loops shapes correspond to the outer edges of these figures. They lie in the xy, yz and zx planes.

As is customary, it is a Monte Carlo simulation using the Metropolis algorithm to generate a Markov chain of gauge field configurations that are distributed according to the Boltzmann weight $\exp(-S)$. Each Monte Carlo step involves randomization of some edge $SU(2)$ matrices, which is done by multiplication of a small $\mathfrak{su}(2)$ algebra matrix, together with a Metropolis step for acceptance/rejection of the update. The algorithm adapted itself to drive the MC acceptance rate towards $1/2$. The use of temporal gauge may slow the convergence of this type of numerical simulation. However, Monte Carlo convergence was ascertained and high quality error estimates were made by the use of data blocking [25]. In addition, convergence was verified subjectively by inspection of the time series for observable values with their accompanying distributions, as well as time series for cumulative averages.

The data blocking error estimates were found to be smaller than the displayed data points in all the plots.

We simulated at different values of β, at each of which we measured the average action density S/N^4, and a list of different Wilson loops shown in Fig. 3, all of which are gauge-invariant quantities. For each Wilson loop shape, we average over all possible loop positions, as well as loop orientations in the xy, yz and zx planes. For a given closed path $\mathcal{C}$, the corresponding Wilson loop variable for gauge group $SU(n)$ is defined as

$$W_{\mathcal{C}} := \frac{1}{2}\Re \operatorname{tr} \prod_{e\in\mathcal{C}} U_e, \tag{23}$$

which involves an ordered product of the edge matrices $\{U_e\}$ along the path $\mathcal{C}$.

Expectation values for any observable quantity $\mathcal{O}$, e.g. the action density S/N^4 or a Wilson loop $W_{\mathcal{C}}$, is given by

$$\langle \mathcal{O} \rangle = \frac{1}{Z} \int \left(\prod_e dU_e \right) \mathcal{O} \exp(-S), \tag{24}$$

where the partition function Z is defined by

$$Z := \int \left(\prod_e dU_e \right) \exp(-S). \tag{25}$$

The integration measure involved in these expressions is a product of the normalized Haar integration measure for each edge group element in the mesh. Note that the normalized Haar measure satisfies

$$\int_{\mathcal{G}} dU = 1. \tag{26}$$

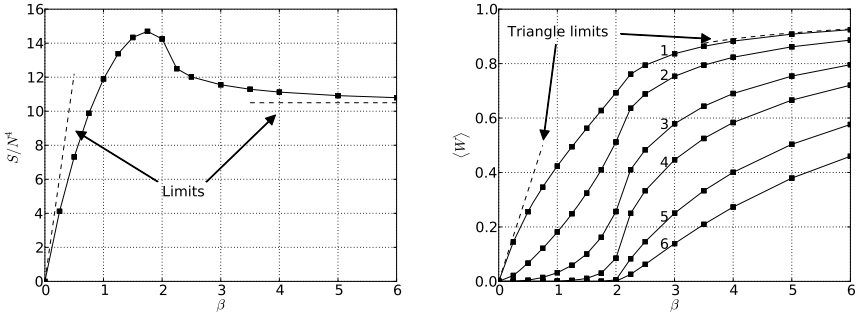

(a) Action density $\langle S/N^4 \rangle$ versus β (b) Wilson loops $\langle W \rangle$ versus β

Fig. 4. Plots showing the β-dependency of (a) the average action density $\langle S/N^4 \rangle$ and (b) the various Wilson loops $\langle W \rangle$ from Fig. 3. Solid squares are data points and solid lines are linear interpolations. The strong and weak coupling asymptotes are included for the action density and the elementary triangular loop. Monte Carlo errors are smaller than the data points.

To accompany these measurements, the strong (small β) and weak (large β) coupling asymptotic behaviour were calculated in Appendix B, using methods described in [6]. At strong coupling, this involves various group integrals, while at weak coupling it suffices to use a thermodynamic analogy to determine the limiting behaviour.

The simulated results for the action density and Wilson loops are displayed in Fig. 4. In Fig. 4(a) we can see the characteristic and nontrivial behaviour in the medium coupling range $\beta \in (1, 3)$. This coincides qualitatively with LGT simulations [26]. Only qualitative, not exact, agreement is expected, since the physical lattice constant will differ in each type of simulation. Compared to LGT simulations, the behaviour at small β deviates more from linearity due to the nonlinear aspects of the SGT action. In this region, the actions do not approximate the continuum action, and differences between discrete actions are unphysical.

The Wilson loops in Fig. 4(b) show the same qualitative behaviour as do LGT simulation results, and approaches the calculated asymptotes nicely. Also here, the behaviour is less linear at small β for the same reason as stated above. The typical strong suppression of the Wilson loops as functions of loop area is reproduced, as expected from the area law behaviour that indicates confinement.

4. Conclusions

We have implemented the general SGT action on a particular simplicial mesh, and performed Monte Carlo quantum field theory simulations that show sensible results that are qualitatively consistent with standard LGT simulations, as must be the case for this initial proof-of-concept implementation.

We expect that this method will lend itself nicely to the use of mesh refinement within quantum QCD simulations, and that this will lead to opportunities of novel applications using nontrivial mesh structures, e.g. in the vicinity of gluon flux tubes as mentioned in the introduction.

The nondiagonal nature of the action increases the amount of computer work in the Metropolis step after each proposed update. However, since the number of interactions for each elementary face is finite, the scaling at large meshes for this model will be the same as for traditional QCD.

There might be possibilities of real-time adaptive diagonalization, thereby increasing the algorithm efficiency throughout the initial part of the simulation.

Acknowledgements

T.G. Halvorsen had funding from SPADE-ACE (Project 176891/V30, The Research Council of Norway). We would like to thank S.H. Christiansen for fruitful discussions.

Appendix A. Simplicial complex, finite elements and mass matrices

Consider a collection of vertexes, edges, faces, tetrahedra in 3d space. These elementary objects are called simplexes, and the collection of these a simplicial complex $\mathcal{T}$. For any k-dimensional simplex T_k for $1 \leqslant k \leqslant 3$, the boundary ∂T_k is a union of $(k-1)$-dimensional simplexes. Consult [27, Section 5.1] for a precise definition. In our construction, we assume that this spatial simplicial complex spans the spatial domain S. The vertexes, edges, faces, and tetrahedra according to dimension, and are labeled i, e, f, and T respectively. The symbol T will be used for simplexes of any dimension.

In order to expand this to a 4d spacetime simplicial complex $\mathbb{T}$, consider a uniform time-discretization with a time spacing Δt. The simplicial complex $\mathcal{T}$ is then repeated at each discrete time step value τ. For each such τ, we define additional simplexes for our $\mathbb{T}$ by extruding each simplex of $\mathcal{T}$ along the time interval $[\tau, \tau + \Delta t]$. As the basic building block in classical 3d FEM theory is a tetrahedron T, the basic building block in this extended FEM version is $T \times I_\tau$, where $I_\tau = [\tau, \tau + \Delta t]$, i.e. a time-extrusion of a tetrahedron. Temporal edges are generated by extruding 3d vertices, and temporal faces by extruding 3d edges.

The space of Whitney k-forms on $\mathcal{T}$ (T) is denoted $W^k(\mathcal{T})$ $(W^k(T))$, with canonical basis (λ_T), T ranging over the set of k-dimensional simplexes in $\mathcal{T}$ [20]. The 0-forms λ_i are the barycentric coordinate maps for each vertex i. In other words, it is the piecewise affine map taking the value 1 at the vertex i and 0 at other vertices. For an edge $e = \{i, j\}$, with orientation $i \to j$, the associated Whitney 1-form is defined by

$$\lambda_e := \lambda_{ij} := \lambda_i \nabla \lambda_j - \lambda_j \nabla \lambda_i. \tag{A.1}$$

For a face $f = \{i, j, k\}$, whose orientation is $i \to j \to k$, the associated Whitney 2-form is defined by

$$\lambda_f := \lambda_{ijk} := 2(\lambda_i \nabla \lambda_j \times \nabla \lambda_k + \lambda_j \nabla \lambda_k \times \nabla \lambda_i + \lambda_k \nabla \lambda_i \times \nabla \lambda_j). \tag{A.2}$$

In the 4d spacetime FEM setting, these basis k-forms are extended to be piecewise affine in time and are denoted $(\Lambda_{T(\tau)})$, i.e.

$$\lambda_T \to \Lambda_{T(\tau)} = \lambda_T \otimes P_1^t,$$

where P_1^t denotes polynomials in the time variable of degree at most one, and $T(\tau) := (\tau, T)$ denotes the spatial simplex T at temporal node τ. More precisely, $\Lambda_{T(\tau)}$ is the piecewise affine function in time, taking the value λ_T at τ and 0 at the other temporal nodes. In addition, we define temporal basis edge and face functions.

To every vertex i in the spatial mesh there are temporal edges $e_t(\tau) = \{i_\tau, i_{\tau+\Delta t}\}$, where $i_\tau := i(\tau)$. The temporal basis edge function attached to $e_t(\tau)$ is then the piecewise constant function in time defined by

$$\Lambda_{e_t(\tau)}(t) = \begin{cases} \lambda_i \circ \pi \frac{1}{\Delta t}\, dt, & t \in [\tau, \tau + \Delta t], \\ 0, & \text{otherwise}, \end{cases}$$

where π is the canonical projection onto the space S,

$$\pi : \mathbb{M} = \mathbb{R} \times S \to S,$$

and dt is the standard basis one-form in the temporal direction.

To every spatial edge e there are corresponding temporal faces $f_t(\tau) = e \times I_\tau$. The temporal basis face function attached to $f_t(\tau)$ is then the piecewise constant function in time defined by

$$\Lambda_{f_t(\tau)}(t) = \begin{cases} \lambda_e \circ \pi \wedge \frac{1}{\Delta t}\, dt, & t \in [\tau, \tau + \Delta t], \\ 0, & \text{otherwise}. \end{cases}$$

In addition to these basis functions, we must define mass matrix elements. Let $m_{TT'}$ denote the classical 3d mass matrices for spatial Whitney elements

$$m_{TT'} = \int_S \lambda_T \cdot \lambda_{T'},$$

where T, T' are k-dimensional simplexes, and $(\cdot)$ denotes the scalar product of alternating forms.

In the definition of the SGT action we use the generalization

$$M_{T(t)T'(\tau)} = \int_{\mathbb{M}} \Lambda_{T(t)} \cdot \Lambda_{T'(\tau)}.$$

This generalization can be expressed through the classical mass matrices by performing the time integration explicitly. Thus, let T be a spatial tetrahedron and $I_\tau = [\tau, \tau + \Delta t]$. Considering now only this time interval, the piecewise affine function taking the value 1 at time τ and 0 at time $\tau + \Delta t$ is given by

$$p_\tau(t) = 1 - \frac{t - \tau}{\Delta t}.$$

The analogous function for the temporal node $\tau + \Delta t$ on the same time interval is given by

$$p_{\tau+\Delta t}(t) = \frac{t - \tau}{\Delta t}.$$

Restricted to the basic building block $T \times I_\tau$, we therefore get

$$M_{f(\tau)f'(\tau)}(T \times I_\tau) = \int_{T \times I_\tau} \Lambda_{f(\tau)} \cdot \Lambda_{f'(\tau)} = \int_{I_\tau} p_\tau^2 \int_T \lambda_f \cdot \lambda_{f'} = \frac{1}{3} \Delta t m_{ff'}(T),$$

$$M_{f(\tau)f'(\tau+\Delta t)}(T \times I_\tau) = \int_{T \times I_\tau} \Lambda_{f(\tau)} \cdot \Lambda_{f'(\tau+\Delta t)} = \int_{I_\tau} p_\tau p_{\tau+\Delta t} \int_T \lambda_f \cdot \lambda_{f'} = \frac{1}{6} \Delta t m_{ff'}(T),$$

$$M_{f(\tau+\Delta t)f'(\tau+\Delta t)}(T \times I_\tau) = \int_{T \times I_\tau} \Lambda_{f(\tau+\Delta t)} \cdot \Lambda_{f'(\tau+\Delta t)} = \int_{I_\tau} p_{\tau+\Delta t}^2 \int_T \lambda_f \cdot \lambda_{f'} = \frac{1}{3} \Delta t m_{ff'}(T).$$

Similarly, the mass matrix element corresponding to the temporal face basis is given by

$$M_{f_t(\tau)f'_t(\tau)}(T \times I_\tau) = \int\limits_{T\times I_\tau} \Lambda_{f_t(\tau)} \cdot \Lambda_{f'_t(\tau)} = \frac{1}{\Delta t}\int\limits_T \lambda_e \cdot \lambda'_e = \frac{1}{\Delta t} m_{ee'}(T).$$

Appendix B. Strong and weak coupling limits

B.1. Strong coupling limit

Here we will show some details regarding the calculation of the strong coupling limits of the elementary triangular Wilson loop. We will use the following integrals over $SU(2)$ group space [6]

$$\begin{aligned} &\int dU\, U^{\alpha\beta} = 0, \qquad \int dU\, U^{\alpha_1\beta_1} U^{\dagger\beta_2\alpha_2} = \frac{1}{2}\delta^{\alpha_1\alpha_2}\delta^{\beta_1\beta_2}, \\ &\int dU\, U^{\alpha_1\beta_1} U^{\alpha_2\beta_2} = \frac{1}{2}\epsilon^{\alpha_1\alpha_2}\epsilon^{\beta_1\beta_2}, \end{aligned} \tag{B.1}$$

where the Greek symbols are matrix indices.

In this calculation, the Wilson loop encircles an elementary spatial triangular plaquette P_t at time t. We denote this Wilson loop by W_{P_t}. By Eq. (23), it is given by

$$W_{P_t} := \frac{1}{2}\Re\,\mathrm{tr}(U_a U_b U_c),$$

where the plaquette P_t is encircled cyclically by the $SU(2)$ edge matrices U_a,U_b and U_c. Due to our choice of distinguished points and plaquette orientations, the spatial SGT action is given by

$$S = \frac{\beta}{2}\sum_{f,f'} M_{ff'}\,\mathrm{tr}\big(U_f U_{f'}^H - U_f - U_{f'}^H + \mathbb{1}\big),$$

where the sum extends over all spatial faces at all times. Since we are interested in small β, consider a first order truncated Taylor expansion of the exponential in Eq. (24), i.e.

$$\langle W_{P_t}\rangle \approx \frac{-\beta}{4Z_\beta}\int\left(\prod_e dU_e\right)\Re\,\mathrm{tr}(U_a U_b U_c)\sum_{f,f'} M_{ff'}\,\mathrm{tr}\big(U_f U_{f'}^H - U_f - U_{f'}^H + \mathbb{1}\big).$$

By the properties of the $SU(2)$ integration measure, terms involving integration over odd powers of link matrices vanish. Therefore, nonvanishing contributions to the integral only come from terms where either f and/or f' coincide with the plaquette P_t. The $U_f U_{f'}^H$ doesn't contribute. Indeed, if either f or f' differ from P_t, we such a term includes an integral over a single power, which vanishes. If on the other hand $f = f' = P_t$, we have $U_f U_f^H = \mathbb{1}$ which again leads to an integral over a single power and thus vanishes. This is also the case for the constant term in the parenthesis.

We are left with

$$\langle W_{P_t}\rangle \approx \frac{\beta}{4Z_\beta}\Re\int\left(\prod_e dU_e\right)\mathrm{tr}(U_a U_b U_c)\sum_{f,f'} M_{ff'}\,\mathrm{tr}\big(U_f + U_{f'}^H\big),$$

where we have moved the real part operator $\Re$ outside of the integral. Contributions only come when at least one of f, f' coincide with P_t. Therefore, by the properties of the particular mesh we have constructed,

$$\langle W_{P_t}\rangle \approx \frac{\beta}{4Z_\beta}(M_{P_tP_t} + M_{P_tP_{t+1}} + M_{P_tP_{t-1}}) \times \Re\int\left(\prod_e dU_e\right)\operatorname{tr}(U_aU_bU_c)\operatorname{tr}\big(U_{P_t} + U_{P_t}^H\big).$$

Using $U_{P_t} := U_aU_bU_c$ and the $SU(2)$ integration formulas (B.1), we get

$$\langle W_{P_t}\rangle \approx \frac{\beta}{2}(M_{P_tP_t} + M_{P_tP_{t+1}} + M_{P_tP_{t-1}}) = \frac{2}{3}\beta,$$

where we have used $Z \approx 1$ for small β. The last equality follows from the particular mass matrix element values produced by our choice of simplicial lattice.

A similar calculation, only slightly more involved because several faces are involved, can be performed to determine the strong coupling limit of the action. Approximations of higher order in β can be found by including higher order terms in the Taylor expansion of the exponential.

B.2. Weak coupling

In order to determine the weak coupling limit of the action density, we simple follow a thermodynamic analogy described in [6]. At large β, the system is described well by a Gaussian partition function approximation. This corresponds to a free theory, and we can find the weak coupling limit of the action by distributing an amount $kT/2 = 1/2\beta$ of energy among all the degrees of freedom in the theory. We have seven edges for each building block cube, each of which contributes three degrees of freedom (the number of generators of $SU(2)$). In accordance with our use of temporal gauge in the simulations, we have excluded the unphysical temporal components when counting degrees of freedom. To obtain the action, we multiply by β, which results in

$$S_{SGT} \to \beta \times \frac{1}{2\beta} \times 7 \times 3 = \frac{21}{2}N^4, \quad \text{as } \beta \to \infty. \tag{B.2}$$

This result can be used to determine the same limit of the triangular Wilson loop in the $\alpha\beta$ plane. We have

$$\langle W_1\rangle = 1 - \frac{a^4}{16}\big\langle\operatorname{tr}\big(F_{\alpha\beta}^2\big)\big\rangle,$$

where there is no sum over the spacetime indices. The antisymmetric field strength has six independent spacetime components. By the equipartitioning of the Euclidean energy among these degrees of freedom, we have

$$\big\langle\operatorname{tr}\big(F_{\alpha\beta}^2\big)\big\rangle = \frac{1}{6}\big\langle\operatorname{tr}\big(F_{\mu\nu}F^{\mu\nu}\big)\big\rangle = \frac{2g^2}{6}\left\langle\frac{S_{SGT}}{N^4}\right\rangle = \frac{42g^2}{12}.$$

Now using $\beta = 2/g^2$, we get

$$\langle W_1\rangle = 1 - \frac{21}{48\beta}. \tag{B.3}$$

Appendix C. Computer implementation

Our computer implementation of the simplicial lattice and accompanying SGT action consists of object-oriented C++ code, using MPICH2 [28] for parallelization, running on a quadruple CPU run-of-the-mill modern workstation computer. The data structures involved are reminiscent of what is used in implementations of the finite element method. This involves different types of mass matrix and connectivity information for elements of the simplicial mesh. The parallelization consisted of running independent simulations on each node, and averaging the results. We used the yarn2 algorithm from the TINA pseudo-random number generator [29], which is designed for use in parallelized algorithms. Although the edge matrix randomization appeared to perform stably enough for our purposes, we regularly did projections of the edge matrices onto $SU(2)$ as a precautionary measure.

References

[1] C.-N. Yang, R.L. Mills, Conservation of isotopic spin and isotopic gauge invariance, Phys. Rev. 96 (1954) 191–195, doi:10.1103/PhysRev.96.191.
[2] S. Weinberg, The Quantum theory of Fields, vol. 1: Foundations, Cambridge Univ. Press, Cambridge, UK, 1995.
[3] S. Weinberg, The Quantum Theory of Fields, vol. 2: Modern Applications, Cambridge Univ. Press, Cambridge, UK, 1996.
[4] M.E. Peskin, D.V. Schroeder, An Introduction to Quantum Field Theory, Addison–Wesley, Reading, USA, 1995.
[5] K.G. Wilson, Confinement of quarks, Phys. Rev. D 10 (8) (1974) 2445–2459, doi:10.1103/PhysRevD.10.2445.
[6] M. Creutz, Quarks, Gluons and Lattices, Cambridge Monographs on Mathematical Physics, Cambridge Univ. Press, Cambridge, UK, 1986.
[7] N.H. Christ, R. Friedberg, T.D. Lee, Weights of links and plaquettes in a random lattice, Nucl. Phys. B 210 (1982) 337, doi:10.1016/0550-3213(82)90124-9.
[8] N.H. Christ, R. Friedberg, T.D. Lee, Gauge theory on a random lattice, Nucl. Phys. B 210 (1982) 310, doi:10.1016/0550-3213(82)90123-7.
[9] N.H. Christ, R. Friedberg, T.D. Lee, Random lattice field theory: General formulation, Nucl. Phys. B 202 (1982) 89, doi:10.1016/0550-3213(82)90222-X.
[10] J.M. Drouffe, K.J.M. Moriarty, C.N. Mouhas, Monte Carlo simulation of pure $U(N)$ and $SU(N)$ gauge theories on a simplicial lattice, Comput. Phys. Commun. 30 (1983) 249, doi:10.1016/0010-4655(83)90092-9.
[11] J.M. Drouffe, K.J.M. Moriarty, C.N. Mouhas, $U(1)$ four-dimensional gauge theory on a simplicial lattice, J. Phys. G 10 (1984) 115, doi:10.1088/0305-4616/10/2/004.
[12] J.M. Drouffe, K.J.M. Moriarty, Gauge theories on a simplicial lattice, Nucl. Phys. B 220 (1983) 253–268, doi:10.1016/0550-3213(83)90040-8.
[13] J.M. Drouffe, K.J.M. Moriarty, $U(2)$ four-dimensional simplicial lattice gauge theory, Z. Phys. C 24 (1984) 395, doi:10.1007/BF01410379.
[14] K.E. Cahill, R. Reeder, Comparison of the simplicial method with Wilson's Lattice Gauge Theory for $U(1)$ in three-dimensions, Phys. Lett. B 168 (1986) 381, doi:10.1016/0370-2693(86)91648-5.
[15] J.M. Drouffe, K.J.M. Moriarty, High-statistics study of the phase transition in $U(2)$ four-dimensional simplicial lattice gauge theory, Journal of Physics G: Nuclear Physics 10 (10) (1984) L221;
URL http://stacks.iop.org/0305-4616/10/i=10/a=001.
[16] R.W.B. Ardill, J.P. Clarke, J.M. Drouffe, K.J.M. Moriarty, Quantum chromodynamics on a simplicial lattice, Phys. Lett. B 128 (1983) 203, doi:10.1016/0370-2693(83)90391-X.
[17] P.G. Ciarlet, The Finite Element Method for Elliptic Problems, 1st edition, Studies in Mathematics and Its Applications, vol. 4, North-Holland Publishing Company, 1978.
[18] P. Monk, Finite Element Methods for Maxwell's Equations, reprinted edition, Oxford Science Publications, 2006.
[19] J.-C. Nédélec, Mixed finite elements in $\mathbb{R}^3$, Num. Math. 35 (1980) 315–341.
[20] H. Whitney, Geometric Integration Theory, Princeton University Press, Princeton, NJ, 1957.
[21] R. Hiptmair, Finite elements in computational electromagnetism, Acta Numerica 11 (2002) 237–339, doi:10.1017/S0962492902000041.
[22] C.M. Bender, K.A. Milton, Approximate determination of the mass gap in quantum field theory using the method of finite elements, Phys. Rev. D 34 (10) (1986) 3149–3155, doi:10.1103/PhysRevD.34.3149.

[23] C.M. Bender, K.A. Milton, D.H. Sharp, Gauge invariance and the finite-element solution of the Schwinger model, Phys. Rev. D 31 (2) (1985) 383–388, doi:10.1103/PhysRevD.31.383.
[24] T.G. Halvorsen, T.M. Sorensen, Simplicial gauge theory on spacetime, arXiv:1107.1420.
[25] H. Flyvbjerg, H.G. Petersen, Error estimates on averages of correlated data, Journal of Chemical Physics 91 (1) (1989) 461–466.
[26] M. Creutz, Monte Carlo study of quantized $SU(2)$ gauge theory, Phys. Rev. D 21 (1980) 2308–2315, doi:10.1103/PhysRevD.21.2308.
[27] S.H. Christiansen, H.Z. Munthe-Kaas, B. Owren, Topics in structure-preserving discretization, Acta Numerica 20 (2011) 1–119, doi:10.1017/S096249291100002X.
[28] MPICH2, URL http://www.mcs.anl.gov/mpi/mpich2.
[29] H. Bauke, TINA pseudo-RNG library, URL http://trng.berlios.de.